REPORT DOCUMENTATION PAGE

Form Approved OMB NO. 0704-0188

1. REPORT DATE (DD-MM-YYYY)	2. REPORT TYPE	3. DATES COVERED (From - To)
15-08-2014	Final Report	1-May-2011 - 30-Apr-2014

4. TITLE AND SUBTITLE
Molecular Engineering of Self-assembled Nanoreactors

5a. CONTRACT NUMBER
W911NF-11-1-0137

5b. GRANT NUMBER

5c. PROGRAM ELEMENT NUMBER
611102

6. AUTHORS
Hao Yan, Yan Liu

5d. PROJECT NUMBER

5e. TASK NUMBER

5f. WORK UNIT NUMBER

7. PERFORMING ORGANIZATION NAMES AND ADDRESSES
Arizona State University
PO Box 876011

Tempe, AZ 85287 -6011

8. PERFORMING ORGANIZATION REPORT NUMBER

9. SPONSORING/MONITORING AGENCY NAME(S) AND ADDRESS (ES)
U.S. Army Research Office
P.O. Box 12211
Research Triangle Park, NC 27709-2211

10. SPONSOR/MONITOR'S ACRONYM(S)
ARO

11. SPONSOR/MONITOR'S REPORT NUMBER(S)
59477-LS.9

12. DISTRIBUTION AVAILIBILITY STATEMENT
Approved for Public Release; Distribution Unlimited

13. SUPPLEMENTARY NOTES
The views, opinions and/or findings contained in this report are those of the author(s) and should not contrued as an official Department of the Army position, policy or decision, unless so designated by other documentation.

14. ABSTRACT
We aim to use molecular engineering to achieve: (1) Rational design and construction of self-assembling DNA nanostructures with the ability to control enzyme encapsulation/release through conformational shifts in the nanostructure in response to environmental changes; (2) Assembly of enzyme and cofactor on a DNA nanostructure to evaluate the essential parameters for modulating catalysis; (3) Switchable enzyme functionality and pathway progression on DNA nanostructures in response to regulator DNA strands. These new technologies integrate the addressability of structural DNA nanotechnology with the functionality of biological enzymes to produce

15. SUBJECT TERMS
DNA nanotechnology, DNA tweezer, Nanoreactor

16. SECURITY CLASSIFICATION OF:			17. LIMITATION OF ABSTRACT	15. NUMBER OF PAGES	19a. NAME OF RESPONSIBLE PERSON
a. REPORT	b. ABSTRACT	c. THIS PAGE			Hao Yan
UU	UU	UU	UU		19b. TELEPHONE NUMBER 480-727-8570

Report Title

Molecular Engineering of Self-assembled Nanoreactors

ABSTRACT

We aim to use molecular engineering to achieve: (1) Rational design and construction of self-assembling DNA nanostructures with the ability to control enzyme encapsulation/release through conformational shifts in the nanostructure in response to environmental changes; (2) Assembly of enzyme and cofactor on a DNA nanostructure to evaluate the essential parameters for modulating catalysis; (3) Switchable enzyme functionality and pathway progression on DNA nanostructures in response to regulator DNA strands. These new technologies integrate the addressability of structural DNA nanotechnology with the functionality of biological enzymes to produce rationally-designed biocatalytic systems based on actuated enzymatic functions.

We have achieved: 1) Development of reliable methods to conjugate DNA to target proteins and attachment of the enzyme cofactors to DNA. These are the fundamental elements required for the spatial self-assembly of multiple enzymes and cofactors on DNA nanostructures. 2) Development of methods to isolate pure DNA-functionalized protein conjugates with exact ratios of DNA:protein. This advance permits precise control over the local organization of the protein-DNA nanostructures assemblies. 3) Development of methods to specifically conjugate DNA oligos to the N- or C- terminus of several dehydrogenases. This advance permits precise control over the position, orientation and the number of conjugated DNA oligos on protein surface as well as maintaining similar enzyme activity as the wild type enzymes. 4) Spatial control of enzyme assembly and subsequent application to studying inter-enzyme substrate diffusion. This elucidated the important spatial parameters for enzyme actuation. 5) Design and construction of responsive DNA nanotweezers with control of inter-component spatial arrangement. The DNA nanotweezers were used to regulate NAD-dehydrogenase activities. 6) Optimization of the regulatory element of DNA nanotweezers to improve their stability and activity. We were able to demonstrate improved closed states of nanotweezers and enzyme activity. 7) Demonstration of the ability of DNA nanocages to encapsulate multi-enzyme cascades. 8) Demonstration of the open and close of DNA nanocages.

Enter List of papers submitted or published that acknowledge ARO support from the start of the project to the date of this printing. List the papers, including journal references, in the following categories:

(a) Papers published in peer-reviewed journals (N/A for none)

Received		Paper
08/15/2014	6.00	D. Han, S. Pal, Y. Yang, S. Jiang, J. Nangreave, Y. Liu, H. Yan. DNA Gridiron Nanostructures Based on Four-Arm Junctions, Science, (03 2013): 0. doi: 10.1126/science.1232252
08/15/2014	7.00	Fei Zhang, Jeanette Nangreave, Yan Liu, Hao Yan. Structural DNA Nanotechnology: State of the Art and Future Perspective, Journal of the American Chemical Society, (08 2014): 11198. doi: 10.1021/ja505101a
08/15/2014	8.00	Jinglin Fu, Yuhe Renee Yang, Alexander Johnson-Buck, Minghui Liu, Yan Liu, Nils G. Walter, Neal W. Woodbury, Hao Yan. Multi-enzyme complexes on DNA scaffolds capable of substrate channelling with an artificial swinging arm, Nature Nanotechnology, (05 2014): 531. doi: 10.1038/nnano.2014.100
08/22/2012	1.00	Minghui Liu, Jinglin Fu, Yan Liu, Neal W. Woodbury, Hao Yan. Interenzyme Substrate Diffusion for an Enzyme Cascade Organized on Spatially Addressable DNA Nanostructures, Journal of the American Chemical Society, (03 2012): 5516. doi: 10.1021/ja300897h
08/22/2012	2.00	Jinglin Fu, Minghui Liu, Yan Liu, Hao Yan. Spatially-Interactive Biomolecular Networks Organized by Nucleic Acid Nanostructures, Accounts of Chemical Research, (08 2012): 1215. doi: 10.1021/ar200295q
08/22/2012	4.00	Andre V. Pinheiro, Dongran Han, William M. Shih, Hao Yan. Challenges and opportunities for structural DNA nanotechnology, Nature Nanotechnology, (11 2011): 763. doi: 10.1038/nnano.2011.187
08/22/2013	5.00	Minghui Liu, Jinglin Fu, Christian Hejesen, Yuhe Yang, Neal W. Woodbury, Kurt Gothelf, Yan Liu, Hao Yan. A DNA tweezer-actuated enzyme nanoreactor, Nature Communications, (07 2013): 0. doi: 10.1038/ncomms3127
TOTAL:		**7**

Number of Papers published in peer-reviewed journals:

(b) Papers published in non-peer-reviewed journals (N/A for none)

Received		Paper
08/22/2012	3.00	Jinglin Fu, Hao Yan. Controlled drug release by a nanorobot, Nature Biotechnology, (05 2012): 407. doi: 10.1038/nbt.2206
TOTAL:	**1**	

Number of Papers published in non peer-reviewed journals:

(c) Presentations

Number of Presentations: 0.00

Non Peer-Reviewed Conference Proceeding publications (other than abstracts):

Received	Paper
TOTAL:	

Number of Non Peer-Reviewed Conference Proceeding publications (other than abstracts):

Peer-Reviewed Conference Proceeding publications (other than abstracts):

Received	Paper
TOTAL:	

Number of Peer-Reviewed Conference Proceeding publications (other than abstracts):

(d) Manuscripts

Received Paper

TOTAL:

Number of Manuscripts:

Books

Received Book

TOTAL:

Received Book Chapter

TOTAL:

Patents Submitted

DNA Gridiron, Inventors: Dongran Han & Hao Yan, Provisional patent filed, 2014.

Patents Awarded

Awards

Hao Yan, Inaugural Milton D. Glick Distinguished Professor, Arizona State University, 01/2012-present
Hao Yan and Yan Liu, The Rozenberg Tulip Award in DNA Computing, 2013

Hao Yan,Member of Editorial Board, Nano Research, 2014 to Present
Hao Yan,Elected President, International Society for Nanoscale Science, Computation and Engineering, 2013
Hao Yan, Finalist, Arizona State University Outstanding Doctoral Mentor Award, 2013
Hao Yan, Member of Editorial Advisory Board, Langmuir, 2011 to Present
Hao Yan, Member of Steering Committee, International Meeting on DNA Computing and Molecular Programming, 2012 to present

Graduate Students

NAME	PERCENT_SUPPORTED	Discipline
Zhao Zhao	1.00	
Shuoxing Jiang	1.00	
Yuhe Yang	1.00	
FTE Equivalent:	**3.00**	
Total Number:	**3**	

Names of Post Doctorates

NAME	PERCENT_SUPPORTED
FTE Equivalent:	
Total Number:	

Names of Faculty Supported

NAME	PERCENT_SUPPORTED	National Academy Member
Hao Yan	0.05	
Yan Liu	0.05	
FTE Equivalent:	**0.10**	
Total Number:	**2**	

Names of Under Graduate students supported

NAME	PERCENT_SUPPORTED	Discipline
Shaun Wooten	0.00	
FTE Equivalent:	**0.00**	
Total Number:	**1**	

Student Metrics

This section only applies to graduating undergraduates supported by this agreement in this reporting period

The number of undergraduates funded by this agreement who graduated during this period: 1.00

The number of undergraduates funded by this agreement who graduated during this period with a degree in science, mathematics, engineering, or technology fields:..... 0.00

The number of undergraduates funded by your agreement who graduated during this period and will continue to pursue a graduate or Ph.D. degree in science, mathematics, engineering, or technology fields:..... 1.00

Number of graduating undergraduates who achieved a 3.5 GPA to 4.0 (4.0 max scale):..... 1.00

Number of graduating undergraduates funded by a DoD funded Center of Excellence grant for Education, Research and Engineering:..... 0.00

The number of undergraduates funded by your agreement who graduated during this period and intend to work for the Department of Defense 0.00

The number of undergraduates funded by your agreement who graduated during this period and will receive scholarships or fellowships for further studies in science, mathematics, engineering or technology fields: 0.00

Names of Personnel receiving masters degrees

NAME
Total Number:

Names of personnel receiving PHDs

NAME
Zhao Zhao
Total Number: 1

Names of other research staff

NAME	PERCENT_SUPPORTED
FTE Equivalent:	
Total Number:	

Sub Contractors (DD882)

Inventions (DD882)

Scientific Progress

See Attachment.

Technology Transfer

None.

Final Report for Grant **W911NF1110137**

Molecular Engineering of Self-assembled Nanoreactors

Principle Investigator: Hao Yan
Co-PI: Yan Liu
Arizona State University

Reporting period: May 01, 2011 to April 30, 2014

I. Scientific and Technical Objectives

Statement of objectives: We aim to use molecular engineering to achieve: (1) Rational design and construction of self-assembling DNA nanostructures with the ability to control enzyme encapsulation/release through conformational shifts in the nanostructure in response to environmental changes; (2) Assembly of enzyme and cofactor on a DNA nanostructure to evaluate the essential parameters for modulating catalysis; (3) Switchable enzyme functionality and pathway progression on DNA nanostructures in response to regulator DNA strands. These new technologies integrate the addressability of structural DNA nanotechnology with the functionality of biological enzymes to produce rationally-designed biocatalytic systems based on actuated enzymatic functions.

II. Approach

Methods employed: We exploited the addressability of DNA nanostructures to organize biological enzymes and evaluate these synthetic biocatalytic systems based on actuated enzymatic functions.

III. Concise Major Accomplishments

We have achieved: 1) Development of reliable methods to conjugate DNA to target proteins and attachment of the enzyme cofactors to DNA. These are the fundamental elements required for the spatial self-assembly of multiple enzymes and cofactors on DNA nanostructures. 2) Development of methods to isolate pure DNA-functionalized protein conjugates with exact ratios of DNA:protein. This advance permits precise control over the local organization of the protein-DNA nanostructures assemblies. 3) Development of methods to specifically conjugate DNA oligos to the N- or C- terminus of several dehydrogenases. This advance permits precise control over the position, orientation and the number of conjugated DNA oligos on protein surface as well as maintaining similar enzyme activity as the wild type enzymes. 4) Spatial control of enzyme assembly and subsequent application to studying inter-enzyme substrate diffusion. This elucidated the important spatial parameters for enzyme actuation. 5) Design and construction of responsive DNA nanotweezers with control of inter-component spatial arrangement. The DNA nanotweezers were used to regulate NAD-dehydrogenase activities. 6) Optimization of the regulatory element of DNA

nanotweezers to improve their stability and activity. We were able to demonstrate improved closed states of nanotweezers and enzyme activity. 7) Demonstration of the ability of DNA nanocages to encapsulate multi-enzyme cascades. 8) Demonstration of the open and close of DNA nanocages.

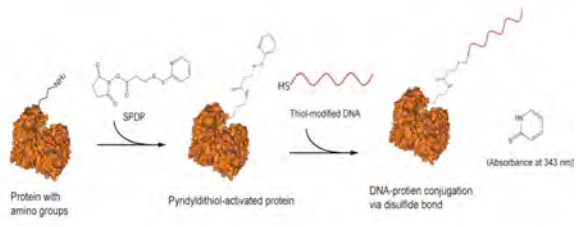

Figure 1. Protein-DNA conjugation using an SPDP crosslinker.

IV. Expanded Major Accomplishments

1. Development of reliable methods to conjugate DNA to target proteins and attachment of the enzyme cofactors to DNA.

1.1. Chemical conjugation strategy for attaching DNA to proteins using SPDP crosslinking chemistry: We developed an SPDP (*N*-Succinimidyl 3-(2-pyridyldithio)-propionate) crosslinking chemistry for attaching oligonucleotides to proteins. As shown in Figure 1, SPDP was used to crosslink GOx and HRP with DNA strands. For a typical conjugation, 100 µl of 40 µM enzyme solution was first reacted with a 20-fold excess of SPDP in 10 mM HEPES buffer (pH 8.5) for one hour, allowing amine-reactive *N*-hydroxysuccinimide (NHS) esters to react with the lysine residues on the protein surface. Excess SPDP was removed by washing, and filtered using Amicon, 30 kD cutoff filters. Next, SPDP-modified protein was conjugated to thiol-modified DNA (10-fold excess) through a disulfide bond exchange of the activated pyridyldithiol group. The reaction mixture was incubated in 1 × PBS (pH 8.5) for two hours. The coupling efficiency was evaluated by monitoring the increase in absorbance at 343 nm due to the release of pyridine-2-thione (extinction coefficient: 8080 M^{-1} cm^{-1}). Finally, the excess DNA was removed by washing, and filtered using Amicon 30 kD cutoff filters. The enzymatic activities of DNA-modified GOx and HRP were ~ 75% of the activities of the unmodified enzymes as shown in Figure 2A. Several DNA-

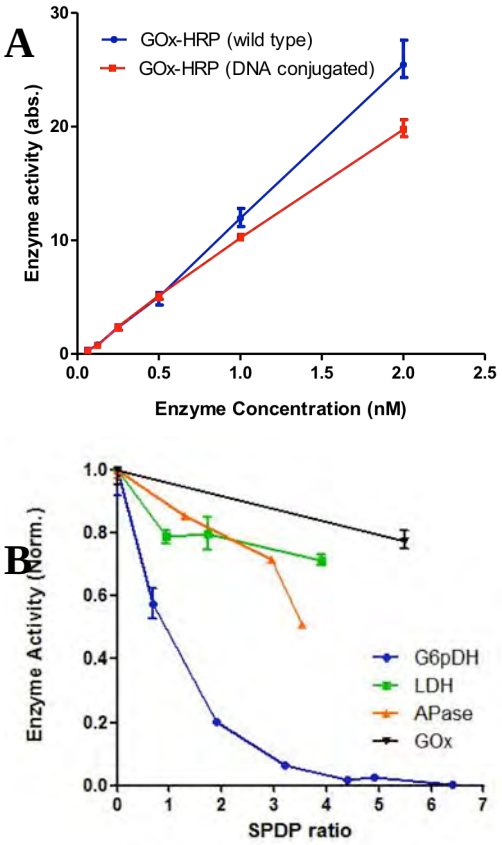

Figure 2. Activities of DNA-protein conjugates (A) Enzyme activity vs. concentration for both DNA-modified GOx/HRP cascades and unmodified enzymes. (B) Activities vs. SPDP ratio for G6pDH, LDH, APase and GOx.

modified enzymes including Glucose 6-phosphate dehydrogenase (G6pDH), Lactate dehydrogenase (LDH), Alkaline Phosphatase (APase) and Glucose Oxidase (GOx), are shown in Figure 2B, comparing the enzyme activities *vs.* the number of SPDP per protein. Over labeling proteins with multiple SPDP results in a reduction in activity, especially for G6pDH.

1.2. Attaching an NAD analogue to DNA: NAD-DNA conjugation is performed on DETE-Sepharose resin (Sigma) where the surfaces are modified with the anion-exchange reactive group diethylaminoethanol (DEAE). In Figure 3A, first, the amino-modified DNA molecule is absorbed onto the positively-charged resin due to strong charge interactions. Then a homogenous disuccinimidyl suberate (DSS) crosslinker is reacted with DNA in DMF with 2% DIPEA for one hour. One succinimidyl ester of DSS reacts with the amino group of the DNA molecule, and forms a covalent amide bond. After this step, the extra DSS is removed by washing the resin with DMF. Second, an amino-modified NAD analogue (AE-NAD) is added to the DNA-resin with 10 fold molar excess and the reaction is incubated in 50 mM HEPES buffer at pH8 for two hours. After this step, the excess NAD is removed by washing the resin with HEPES buffer. Finally, the NAD-DNA absorbed on the resin surfaces is collected by

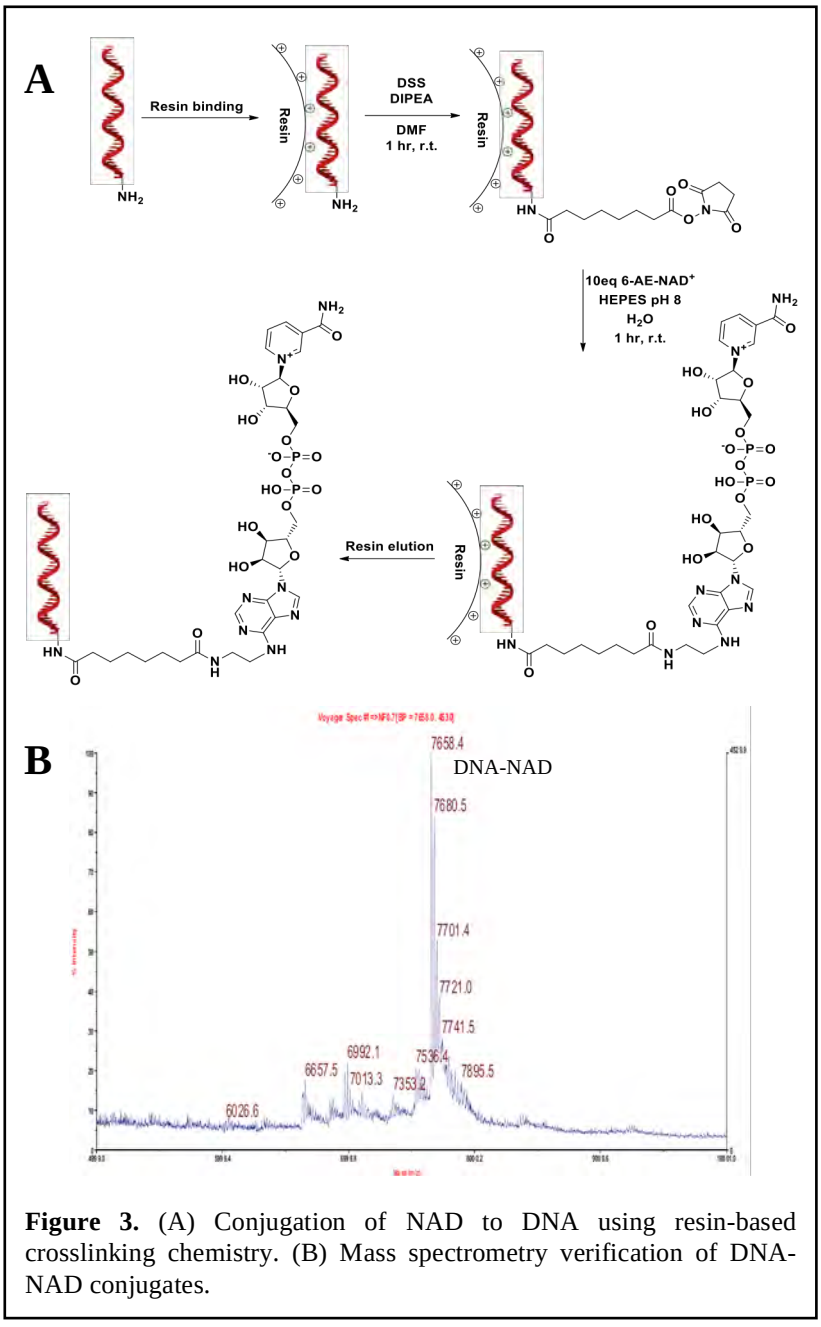

Figure 3. (A) Conjugation of NAD to DNA using resin-based crosslinking chemistry. (B) Mass spectrometry verification of DNA-NAD conjugates.

adding high concentration NaCl (1.5 M) to compete off the DNA from the DEAE-modified resin. The collected DNA-NAD mixture is further purified using HPLC. Figure 3B shows the mass spectrometry characterization of the DNA-NAD conjugate.

We further tested the thermal stability of the NAD and amino-modified NAD analogue (AE-NAD) as shown in Figure 4. The thermal tests showed that NAD and AE-NAD maintained their activity when incubated at temperatures less than 75 ˚C. This result revealed the ideal conditions for annealing NAD with the DNA nanostructures.

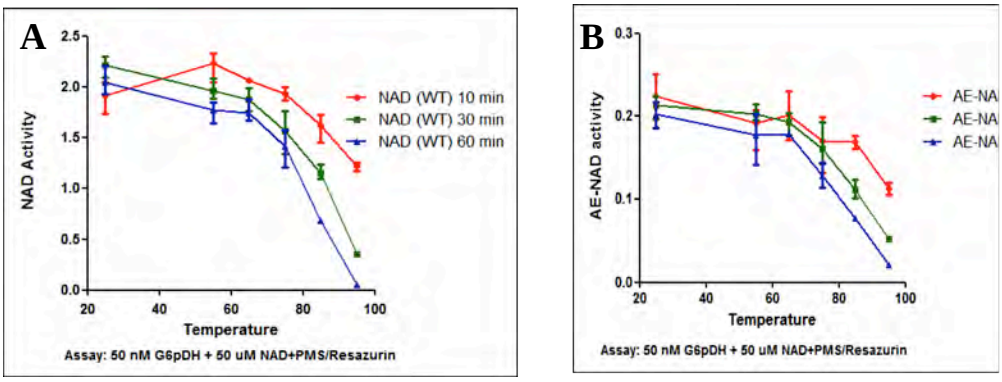

Figure 4. Thermal stability of NAD (A) and amino-modified NAD (B).

2. Development of methods to isolate pure DNA-functionalized protein conjugates with exact ratios of DNA:protein.

After the SPDP (*N*-Succinimidyl 3-(2-pyridyldithio)-propionate) crosslinking chemistry for attaching oligonucleotides to proteins as shown in Figure 1, the excess DNA is removed by filtration with Amicon-30 kD cutoff filters, followed by a single wash with 100 mM HEPES (pH 7.4) containing 1 M NaCl and three consecutive washes with 1×PBS (pH 7.4). The high salt concentration in the first buffer helps to remove

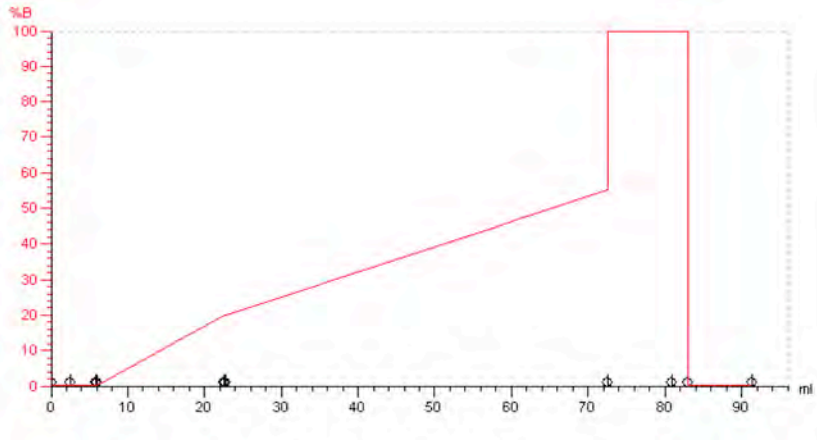

Figure 5. Elution gradient for anion-exchange chromatography. Buffer A: 50 mM sodium phosphate (pH 7.5); buffer B: 50 mM sodium phosphate and 1 M NaCl (pH 7.5).

nonspecifically bound DNA from the surface of the protein. MDH-oligo conjugates are washed one additional time with 10 mM HEPES containing 150 mM NaCl and 0.05% (v/v) P-20 detergent to remove nonspecifically absorbed DNA from the surface of the proteins.

To achieve more accurate control over the conformation and assembly of the protein-DNA nanostructures required that we develop a method to purify DNA functionalized proteins with different numbers of DNA molecules per protein. Figure 5 shows the purification of DNA conjugated protein by ionic-exchanged fast protein liquid chromatography (FPLC). 500 ul of 50 µM G6pDH-TTTTTCCCTCCCTCC, with an average ratio of ~ 2 DNA molecules per protein, was loaded onto an anion exchange column in the FPLC using an elution gradient of 20% 50 mM sodium phosphate (1 M NaCl) to 55% 50 mM sodium phosphate (1 M NaCl) (Figures 5 and 6). Multiple peaks from the corresponding chromatogram were collected, including unmodified protein, protein functionalized with 1 DNA, protein functionalized with 2 DNAs, protein functionalized with 3 DNAs, protein functionalized with 4 DNAs and free DNA molecules.

Due to presence of multiple lysine residues on the surface of both proteins, the reaction products are mixtures of unique conjugates with different number of DNAs attached (even for conjugates with the same number of DNAs, the site of labeling can also vary). To isolate enzymes modified with different numbers of DNA oligonucleotides, the DNA-functionalized proteins described above were then purified by anionic-exchange chromatography using AKTA fast-protein liquid chromatography (FPLC, GE Healthcare). For a typical purification, ~ 500 µL of 50 µM G6pDH-P1 solution, with an average of ~ 1.5 DNA molecules per protein, was loaded onto an FPLC in an anion exchange column (MonoQ 4.6/100 PE, GE Healthcare) using an elution gradient (Figure

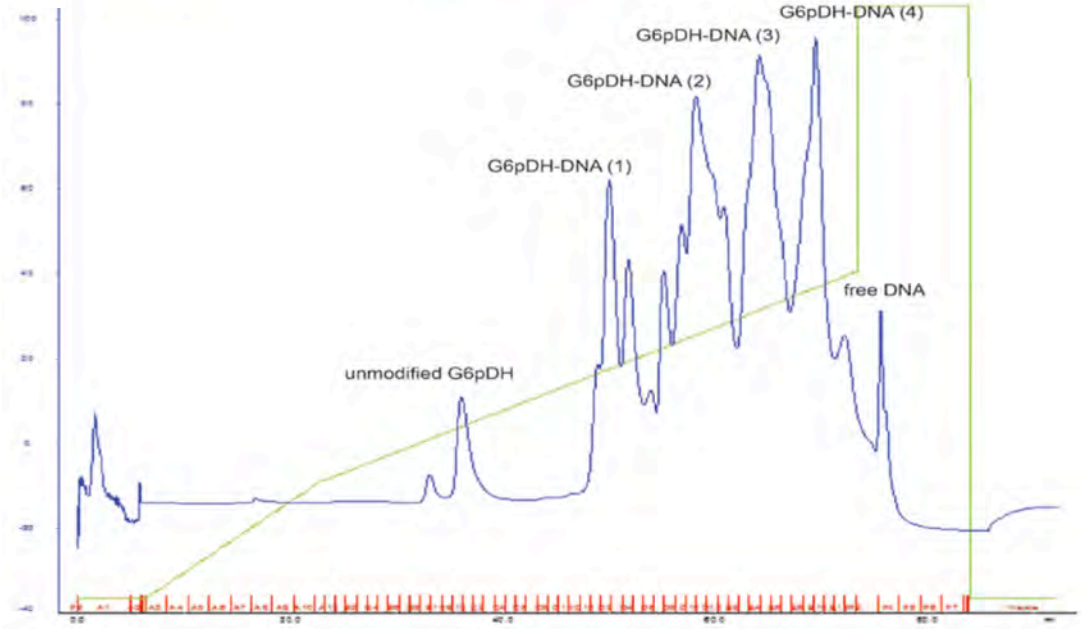

Figure 6. Anion-exchange FPLC for purification of G6pDH-DNA conjugates. The proteins with different numbers of DNA molecules attached were separated into distinct fractions that were collected. Condition: buffer A, 50 mM sodium phosphate (pH7.5); buffer B, 50 mM sodium phosphate, 1 M NaCl (pH 7.5). The identities of the distinct peaks were assigned using the A260 and A280 data (Table 1).

2) from 20% 50 mM sodium phosphate (1 M NaCl) to 55% 50 mM sodium phosphate (1 M NaCl) and a 1.5 mL/min flow rate.

Multiple peaks from the chromatogram were collected and were identified as unmodified proteins, proteins with 1, 2, 3 and 4 DNA molecules attached, and free DNA molecules, respectively (Figure 6). The fractions were subsequently concentrated using Amicon-30 kD cutoff filters. To calculate the number of DNA molecules per protein, we measured and compared the absorbance of the conjugates at 260 and 280 nm (Table 1).

DNA	A260/A280	ε_{260} (M^{-1} cm^{-1})	ε_{260} (M^{-1} cm^{-1})	Protein	A260/A280	ε_{260} (M^{-1} cm^{-1})	ε_{260} (M^{-1} cm^{-1})	FPLC Fractions	A260/A280	A260	A280	DNA - to-Protein Ratio	Protein Conc. (uM)
P-1	1.27	115200	90709	**G6pDH**	0.52	61594	118450	D1-D5	0.86	1.28	1.49	1.08	6.88
P-1	1.27	115200	90709	**G6pDH**	0.52	61594	118450	D9-E2	0.96	6.651	6.90	1.89	23.80
P-1	1.27	115200	90709	**G6pDH**	0.52	61594	118450	E3-E7	1.03	8.557	8.30	2.80	22.29
P-1	1.27	115200	90709	**G6pDH**	0.52	61594	118450	E8-E11	1.08	6.855	6.34	3.88	13.47

Table 1. Determining the concentration and number of DNA molecules in purified G6pDH-DNA (P-1) and MDH-DNA (P-2) conjugates by measuring the absorbance at 260 and 280 nm and using the following equations:

A_{260} (DNA-protein) = ε_{260} (protein) *Conc.(protein) + ε_{260} (DNA)*Conc.(DNA)

A_{280} (DNA-protein) = ε_{280} (protein) *Conc.(protein)+ ε_{280} (DNA)*Conc.(DNA)$A_{260}(\text{DNA-protein}) = \varepsilon_{260}(\text{protein})*\text{Conc.}(\text{protein}) + \varepsilon_{260}(\text{DNA})*\text{Conc.}(\text{DNA})$

Ratio(DNA/protein)=(Conc.(DNA))/(Conc.(protein))

The activities of pure, DNA functionalized dehydrogenase enzymes were evaluated for their dependence on the number of attached DNA molecules, as shown in Figure 7.

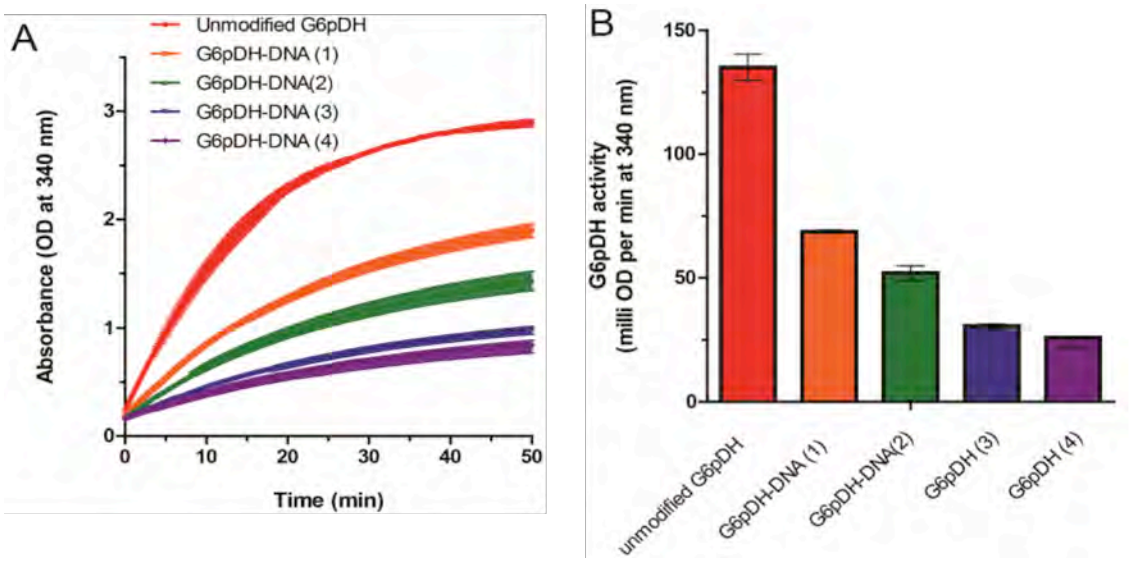

Figure 7. Stoichiometric dependence of the activity of DNA-conjugated dehydrogenases on the number of DNA molecules displayed from their surface. (A-B) G6pDH-DNA conjugates with 0, 1, 2, 3 and 4 DNA molecules, collected from FPLC. Assay condition: 2 nM G6pDH-DNA conjugates with 1 mM G6p and 1 mM NAD+ in 100 mM HEPES (pH 8)

G6pDH labeled by two DNA molecules maintained ~ 40 % activity of the wild type, while enzymes with 3 or 4 DNA molecules exhibited significantly lower activities.

3. Development of methods to specifically conjugate DNA oligos to the N- or C-terminus of several dehydrogenases.

3.1. Gene cloning into Halo-tag vectors and protein expression

Due to the presence of multiple lysine residues on the surface of both Glucose-6-phosphate dehydrogenase (G6pDH) and Malate dehydrogenase (MDH), the reaction products are mixtures of unique conjugates with different numbers of DNAs attached, if using the SPDP crosslinking chemistry. To isolate enzymes modified with different

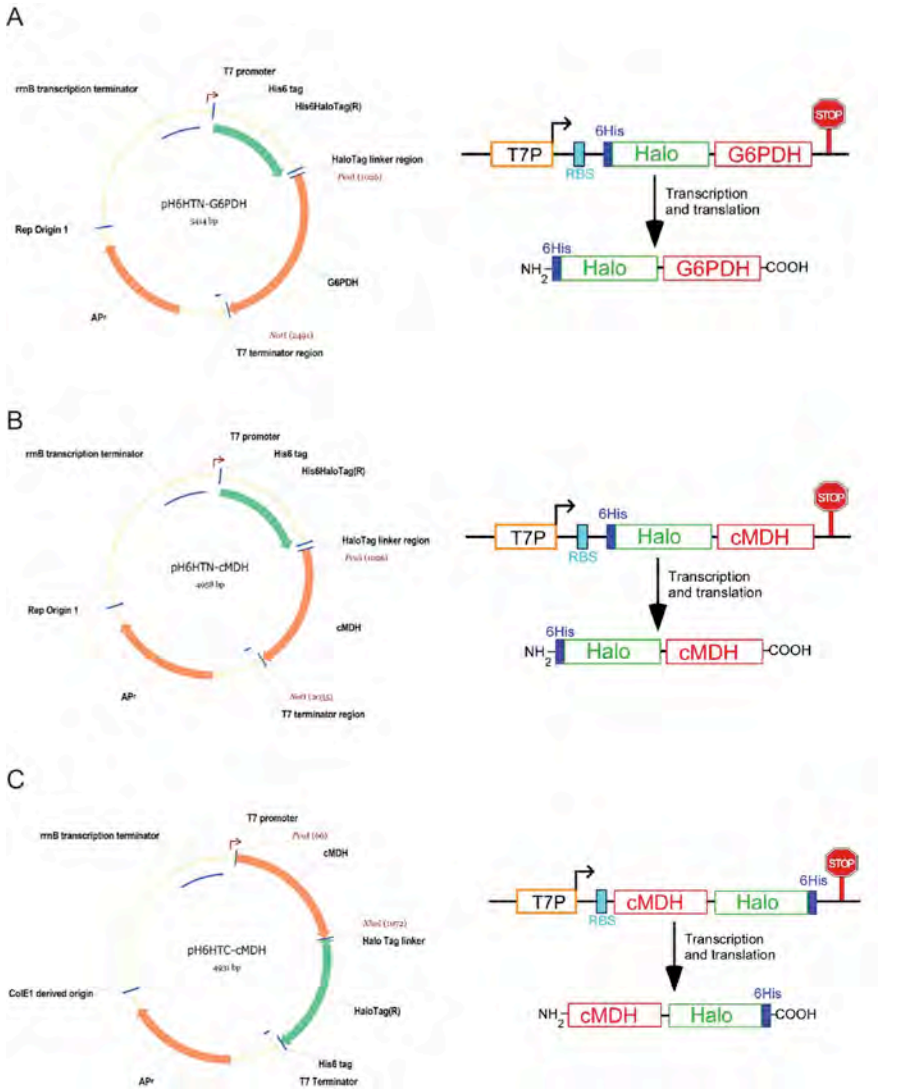

Figure 8. Schematics of enzyme gene cloning into Halo-tag vectors. DNA sequences encoding G6pDH and MDH were cloned into pH6HTN vector for N-terminal modification or pH6HTC for C-terminal modification. After transcription and translation, Halo-tagged proteins can be obtained with modification at either N- or C- terminus. (A) Map of fused Halo-G6pDH gene construct (left) and expression flow of N-terminal tagged G6pDH (right); (B) MDH fused with N-terminal Halo tag; (C) MDH fused with C-terminal Halo tag.

numbers of DNA oligonucleotides, we developed a purification method using anionic-exchange chromatography by AKTA fast-protein liquid chromatography (FPLC, GE Healthcare) (Fig. 11A). However, the SPDP reaction randomly labels surface lysine residues, and decreases the activity of some enzymes after conjugation if the lysine residues at active sites are modified. Additionally, it lacks precise control over the position, orientation and the number of modified DNA oligos. Here, we have developed a method to specifically conjugate DNA oligos to the N- or C- terminus of several dehydrogenases.

To achieve more accurate control over DNA- protein conjugation site specificity we developed a technique to conjugate DNA oligos to the N- or C- terminus of G6pDH and MDH. Figure 8 shows the method for cloning genes into Halo-tag vectors. The amino acid sequences of Glucose 6-phosphate dehydrogenase (G6PDH) and cytosolic malate dehydrogenase (cMDH) were obtained from GenBank with the accession numbers AAA25265 and NP_999039, respectively. DNA sequences encoding for these two proteins were purchased from Genscript with codons optimized for *E. coli* expression. The *G6PDH* and *cMDH* genes were digested with the restriction enzymes PvuI and NotI (New England Biolabs) and cloned into the pH6HTN vector (Promega) digested by the same enzymes. For the cloning of *cMDH* into the C-terminal Halo tag vector pH6HTC, both *cMDH* and pH6HTC were cleaved using PvuI and XhoI and purified. Ligation reactions were performed by mixing the digested gene and vector with a 3:1 molar ratio in 1X ligation buffer and 1U T4 DNA ligase (New England Biolabs) at room temperature for 2 hours. Ligation products were transformed into the NEB 5-alpha competent cells

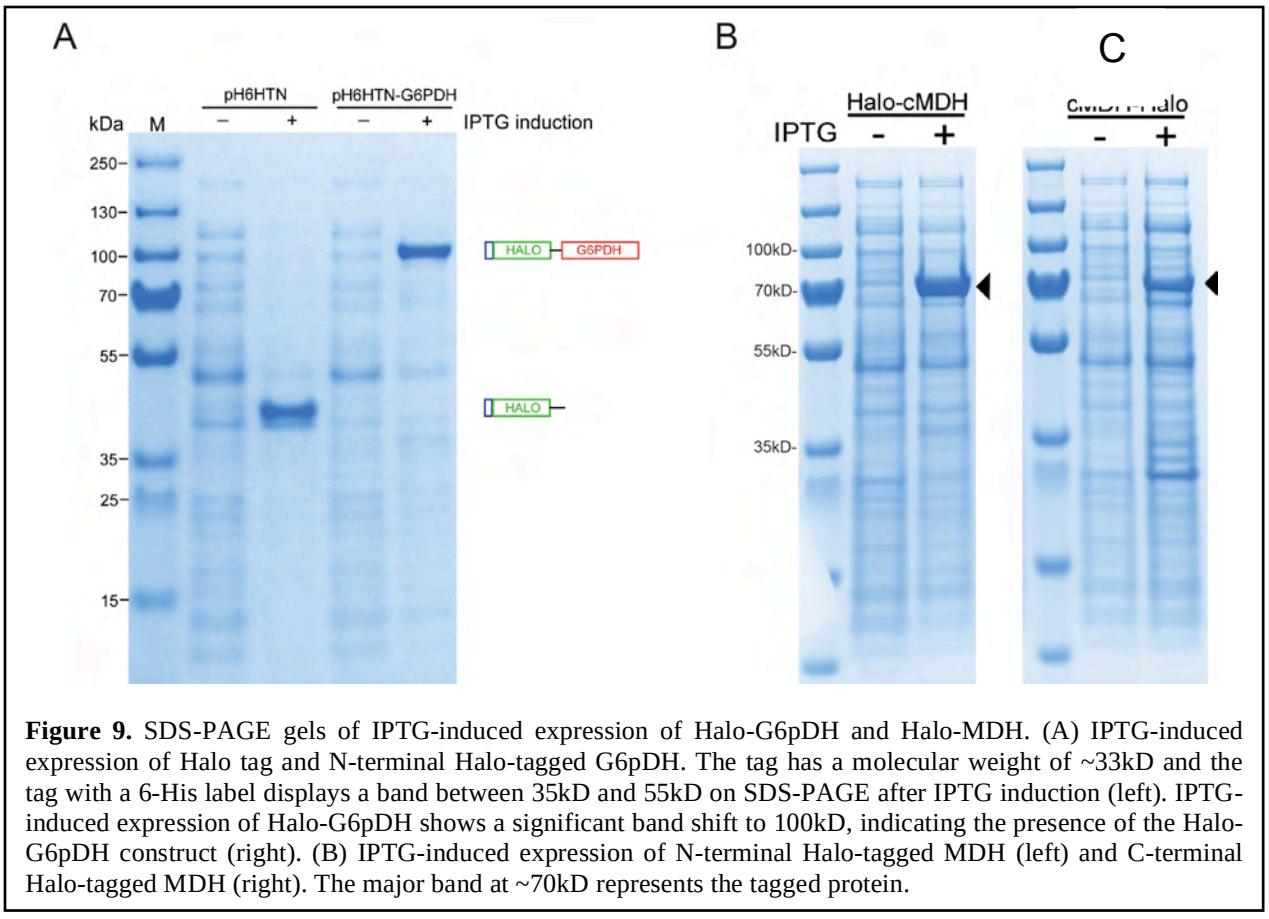

Figure 9. SDS-PAGE gels of IPTG-induced expression of Halo-G6pDH and Halo-MDH. (A) IPTG-induced expression of Halo tag and N-terminal Halo-tagged G6pDH. The tag has a molecular weight of ~33kD and the tag with a 6-His label displays a band between 35kD and 55kD on SDS-PAGE after IPTG induction (left). IPTG-induced expression of Halo-G6pDH shows a significant band shift to 100kD, indicating the presence of the Halo-G6pDH construct (right). (B) IPTG-induced expression of N-terminal Halo-tagged MDH (left) and C-terminal Halo-tagged MDH (right). The major band at ~70kD represents the tagged protein.

(New England Biolabs) and the correct clones were confirmed by DNA sequencing. Plasmids pH6HTN-G6PDH and pH6HTN-cMDH were then transformed into NEB T7 express LysY competent cells (New England Biolabs). A single colony was inoculated into 10 ml LB medium and grown at 37°C with constant shaking overnight. The 10 mL overnight culture was then inoculated into 1 L LB medium and incubated in a 37°C shaking incubator. Isopropyl-β-D-thiogalactopyranoside (IPTG) was added to yield a final concentration of 0.5 mM after the OD600 reached 0.6. *E. coli* cells were harvested 3 hours after IPTG induction by centrifugation at 7,000xg for 15 min. Cells were then resuspended in 20 ml of lysis buffer (20 mM Sodium Phosphate pH 7.5, 0.5 M NaCl, 20 mM imidazole and 0.3 mM TCEP supplemented with 1X Complete Protease Inhibitor Cocktails [Roche Diagnostics]) and lysed with sonication. The cell lysate was clarified by centrifugation at 20,000xg for 30 min at 4°C and the supernatant was filtered through a 0.22 μM membrane. The 6XHis-tagged Halo fusion proteins were purified with Histrap HP chromatography under the manufacturer's instructions (GE Healthcare). The elution fractions were analyzed by 4-15% Mini-PROTEAN TGX Stain-free SDS-PAGE gels. Different fractions containing the desired proteins were pooled and selected for DNA conjugation. Figure 9 shows IPTG-induced expression of Halo-G6pDH and Halo-MDH.

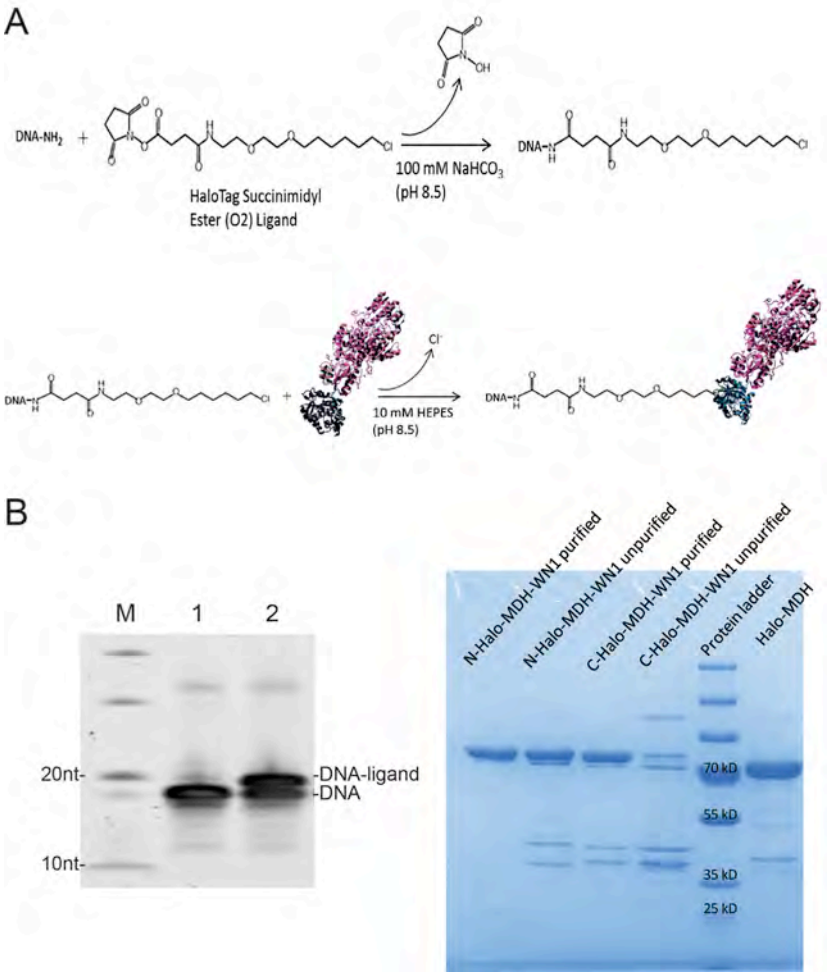

Figure 10. Site-specific Halo-tagged protein-DNA conjugation. (A) General scheme; (B) 14% denaturing gel of unmodified single-stranded DNA (ssDNA, lane 1) and ssDNA-ligand conjugates (lane 2), yield is estimated to be ~50% from band intensity. (C) SDS PAGE of wildtype Halo-MDH and N-terminal Halotagged MDH conjugated with WN1 (DNA strand) and C-terminal Halotagged MDH conjugated with WN1.

3. 2. Conjugating DNA to Halo-tagged protein

The scheme of conjugating DNA specifically to Halo tag is shown in Figure 10A. In the first step, 100 µL of 10 mM HaloTag ® Succinimidyl Ester (O2) Ligand (purchased form Promega) was prepared in DMSO. 500 µL of 100 µM 5'amine-modified oligo (WN1 sequence: TTTTTCCTCCCTCC) was incubated with 20-fold excess of the Halotag ligand in 100 mM $NaHCO_3$ (pH 8.5) for 2h. After this reaction, excess Halotag-ligand was removed by washing with 3 kD cutoff Amicon filters. Halotag-ligand conjugated DNA was characterized by 14% denaturing PAGE as shown in Figure 8B. The reaction yield was estimated to be ~50% from the band intensity between ssDNA and ssDNA-ligand conjugates. In the second step, 500 µL of 40 µM enzyme solution was incubated with DNA-ligand conjugates in 10 mM sodium HEPES (pH 8.5) at room temperature for one hour, allowing the halotag ligand to react with the Halo-tagged protein, forming a covalent DNA-protein linkage. In this reation, a 2-fold excess of ssDNA-ligand was used to produce Halo-G6pDH-DNA, while a 4-fold excess of ssDNA-ligand was used to conjugate Halo-MDH-DNA.

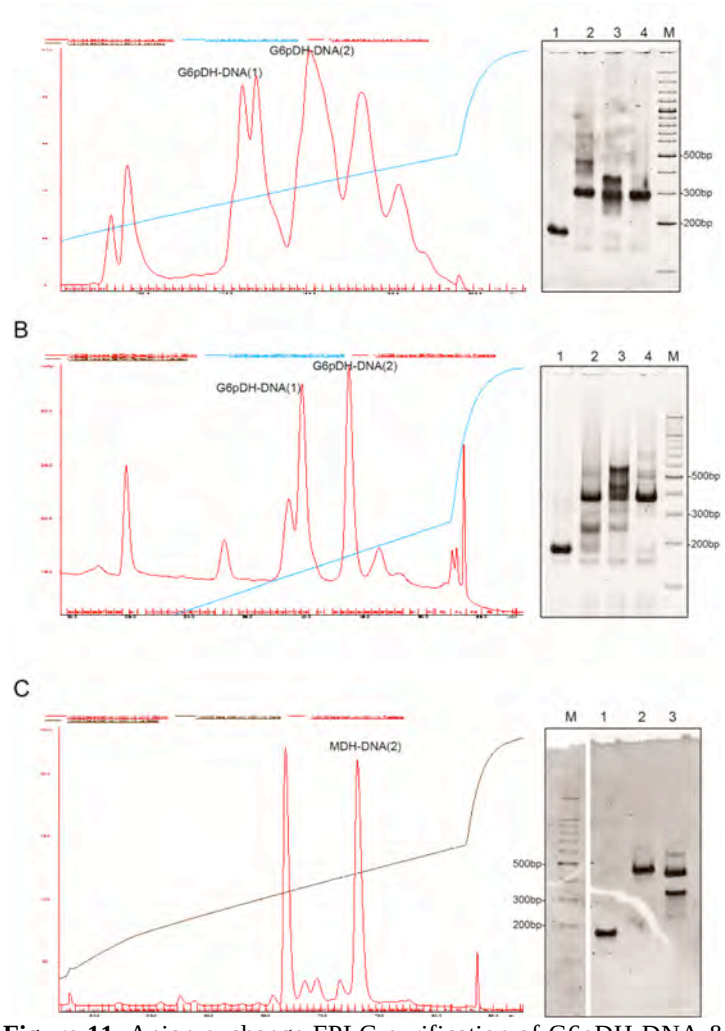

Figure 11. Anion-exchange FPLC purification of G6pDH-DNA & MDH-DNA conjugates and native gel characterization of the DNA tile-protein assembly. SPDP cross-linked G6pDH-DNA conjugates (A) and Halotagged G6pDH-DNA conjugates (B). Lane 1 to 4 of 3% native gel: DNA tile, tile assembled with unpurified G6pDH-DNA, tile assembled with purified G6pDH labeled with 1 DNA, and tile assembled with purified G6pDH labeled with 2 DNA; (C) Halotagged MDH-DNA conjugates. Lane 1 to 3: DNA tile, tile assembled with purified N-Halo MDH labeled with 2 DNA and tile assembled with purified C-Halo MDH labeled with 2 DNA. Condition: buffer A, 50 mM sodium phosphate (pH7.5); buffer B, 50 mM sodium phosphate, 1 M NaCl (pH 7.5).

To isolate enzymes modified with an exact number of oligonucleotides, the Halo-tagged protein-DNA conjugates obtained in the above procedures were purified with anionic-exchange chromatography using ionic-exchanged FPLC (using the same buffer and gradient as described above in the purification method for SPDP conjugation). The purification results are shown in Figure 11B (G6pDH) and C (MDH). Two peaks from

the corresponding chromatograms were collected, yielding each protein functionalized with one or two DNA oligos. The filtered protein-oligo solution was quantified by absorbance at 260 and 280 nm (Table 2).

DNA	A260/A280	ε_{260} (M^{-1} cm^{-1})	ε_{280} (M^{-1} cm^{-1})	Protein	A260/A280	ε_{260} (M^{-1} cm^{-1})	ε_{280} (M^{-1} cm^{-1})	Conjugates	A260/A280	A260	A280	DNA - to-Protein Ratio	Protein Conc. (uM)
WN1	1.27	115200	90709	N teminal Halo-MDH	0.71	131677	185460	wildetype	0.71	4.95	7.00	0.00	37.94
WN1	1.27	115200	90709	N teminal Halo-MDH	0.71	131677	185460	labeled with DNA	0.91	4.95	5	1.11	19.11

Table 2. Determining the concentration and number of DNA molecules in N-terminal Halo-MDH-DNA conjugates by measuring the absorbance at 260 and 280 nm and using the following equations:

$$A_{260}\,(\text{DNA-protein}) = \varepsilon_{260}\,(\text{protein})\,{*}\text{Conc.(protein)} + \varepsilon_{260}\,(\text{DNA}){*}\text{Conc.(DNA)}$$

$$A_{280}\,(\text{DNA-protein}) = \varepsilon_{280}\,(\text{protein})\,{*}\text{Conc.(protein)} + \varepsilon_{280}\,(\text{DNA}){*}\text{Conc.(DNA)}$$

$$A_{260}(\text{DNA-protein}) = \varepsilon_{260}(\text{protein}){*}\text{Conc.}\,(\text{protein}) + \varepsilon_{260}(\text{DNA}){*}\text{Conc.}\,(\text{DNA})$$

$$\text{Ratio(DNA/protein)} = (\text{Conc.(DNA)})/(\text{Conc.(protein)})$$

Assembly of the different DNA:protein conjugates protein on DNA tiles depending on labeled DNA molecules per protein for Halo-G6pDH-WN1 and Halo-MDH-WN1 were evaluated by 3% native PAGE (Fig. 11). Halo-G6pDH and Halo-MDH labeled with two DNA molecules gave the correct assembly of one protein per DNA structure with more than 90% yield. Both enzymes labeled with one DNA molecule per protein resulted in lower assembly yield and dimeric assembly.

3.3 Evaluating the enzymatic activity of site specific DNA-protein conjugates:

The activities of purified Halotagged protein conjugated with 1 and 2 oligos were

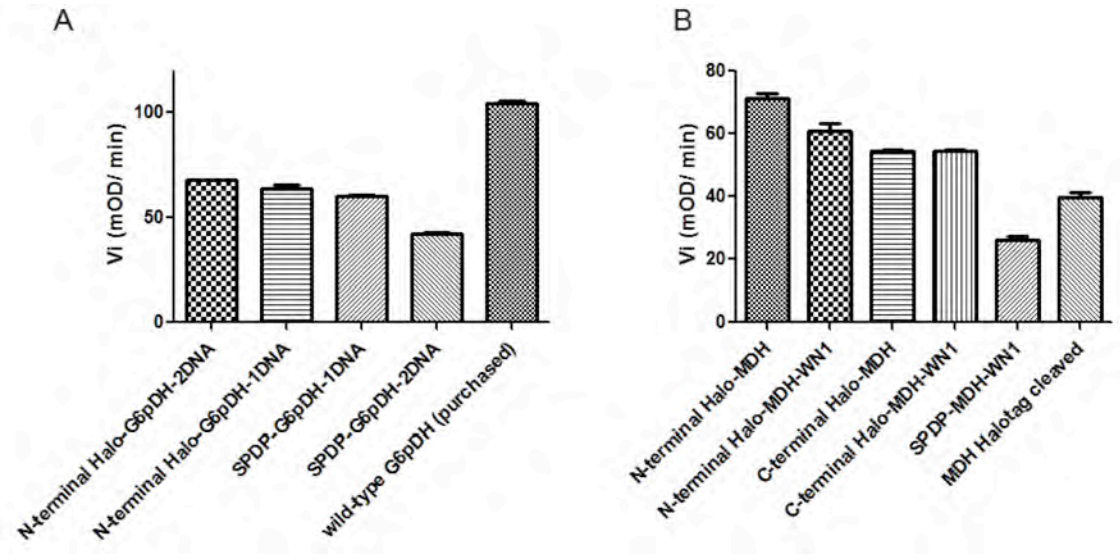

Figure 12. Activity comparison of SPDP DNA-protein conjugation and halotagged protein-DNA conjugation of G6pDH and MDH. (A) The activity of G6pDH-DNA conjugates compared with wildtype G6pDH purchased from Sigma. (B) The activity of MDH-DNA conjugates compared with wildtype MDH. Assay condition: 2 nM G6pDH-DNA conjugates with 1 mM G6p and 1 mM NAD+ in 100 mM HEPES (pH 8); 2 nM MDH-DNA conjugates with 1 mM OAA and 1 mM NADH in 100 mM HEPES (pH 8).

evaluated and compared with the activities of SPDP modified protein with 1 and 2 DNAs, as shown in Figure 12. Halo-G6pDH labeled with 2 DNA molecules has 1.5 fold activity of the SPDP-G6pDH, while Halo-G6pDH labeled with 1 DNA molecule has similar activity of the SPDP-G6pDH. N-terminal Halo-MDH labeled with 2 oligos has ~ 3 fold activity enhancement compared to SPDP labeled MDH. For both dehydrogenases we tested here, Halotagged dehydrogenases retained activity when labeled with multiple DNAs, while SPDP labeled dehydrogenases activity decreased significantly when labeled DNA molecules increases.

4. Spatial control of enzyme assembly and subsequent application to studying inter-enzyme substrate diffusion.

We demonstrated spatial control of the GOx/HRP cascade organized by DNA origami structures. As shown in Figure 13, the distance between GOx and HRP was varied from 10 nm, 20 nm, 45 nm to 65 nm with high assembly yield. Atomic Force Microscopy (AFM) was used to quantify the level of protein assembly on the DNA origami tiles - assembled enzymes exhibited higher surface landscapes than the underlying origami tiles.

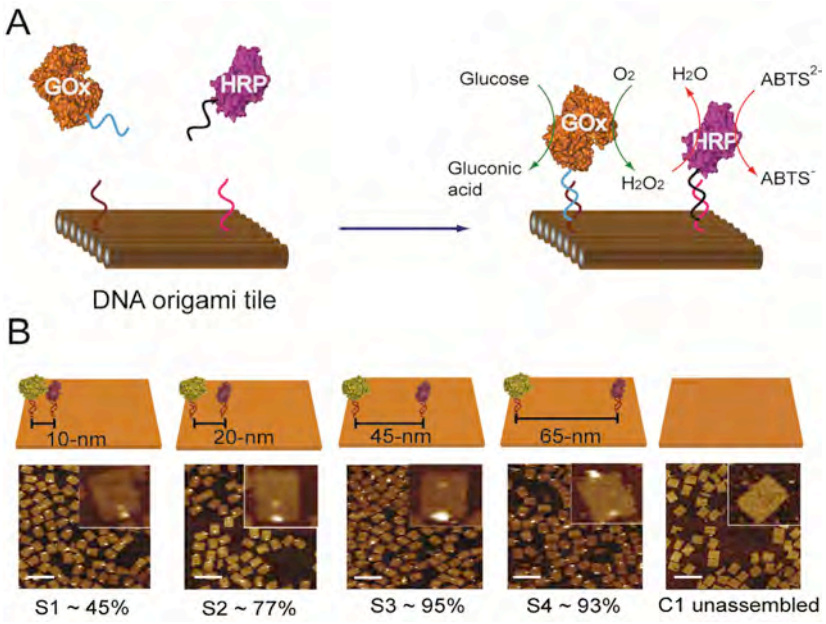

Figure 13. DNA nanostructure-directed co-assembly of GOx and HRP enzymes. (A) The assembly strategy and details of the GOx/HRP enzyme cascade. (B) Rectangular DNA origami tiles with assembled Gox/HRP pairs with inter-enzyme distances ranging from 10 nm to 65 nm. GOx/HRP co-assembly yields were determined from AFM images as shown in the bottom panel. Scale bar: 200 nm.

As shown in Figure 14, we proceeded to investigate the overall activities of the GOx/HRP cascades as a function of inter-enzyme distance. The study revealed two different distance dependent kinetic processes associated with the assembled enzyme pairs. Strongly enhanced activity was observed for those assemblies in which the enzymes were closely spaced, while the activity dropped dramatically for enzymes > 20 nm apart. Increasing the inter-enzyme distance further resulted in much weaker distance dependence. Combined with diffusion modeling, the results suggest that Brownian diffusion of intermediates in solution governed the variations in activity for more distant enzyme pairs, while dimensionally-limited diffusion of intermediates across connected protein surfaces contributed to the enhancement in activity for closely spaced GOx/HRP assemblies.

To further test the role of limited dimensional diffusion along protein surfaces, a noncatalytic protein bridge was inserted between GOx and HRP (connecting their hydration shells). This resulted in substantially enhanced activity of the enzyme pair. In Figure 15, we depict a 'bridge-based' cascade in which a non-catalytic protein that was intended to connect the protein hydration shells and facilitate the surface-limit diffusion of H_2O_2 was inserted between GOx and HRP. As shown in Figure 15A, a GOx/HRP pair was first assembled on a DNA origami tile with a 30 nm inter-enzyme distance. Next, a non-catalytic protein, either neutravidin (NTV) or streptavidin (STV)-conjugated β-galactosidase (β-Gal), was inserted between the enzymes. As shown in Figure 15B, assembled GOx/HRP pairs with a β-Gal bridge exhibited ~ 42 ± 4% higher raw activity than control assemblies without the bridge. For

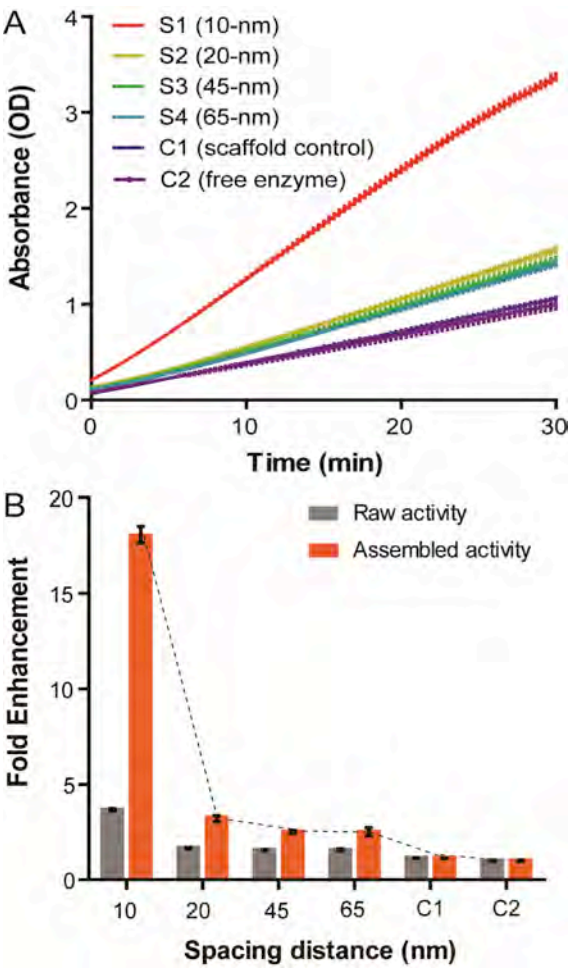

Figure 14. Inter-enzyme distance-dependence of assembled GOx/HRP pairs as illustrated by (A) plots of product concentration vs. time for various nanostructured and free enzyme samples and (B) enhancement of the activity of the enzyme pairs on DNA nanostructures compared to free enzymes in solution. Both the raw activity (uncorrected for the yield of the completely assembled nanostructures) and yield-corrected activity are shown. GOx/HRP co-assembly yields were determined from AFM images.

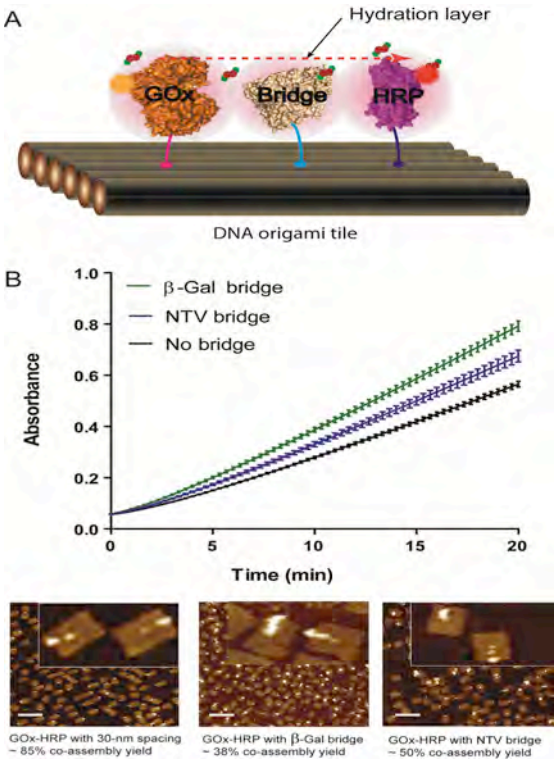

Figure 15. Surface-limited H_2O_2 diffusion induced by a protein bridge. (A) The design of an assembled GOx/HRP pair with a protein bridge used to connect the hydration surfaces of the enzymes. (B) Enhancement in the activity of assembled GOx/HRP pairs with β-Gal and NTV bridges compared to un-bridged GOx/HRP pairs. AFM images of GOx/HRP pairs with and without protein bridges were used to estimate the co-assembly yield. Scale bar: 200 nm.

this preparation, the yield of assemblies with all three components (GOx, HRP and the bridge) was ~ 38%. Assembled GOx/HRP pairs with a NTV bridge showed ~ 20 ± 4% enhancement in raw activity compared to the control sample, at ~ 50% co-assembly yield. STV conjugated β-Gal and NTV in solution did not affect GOx/HRP activities. With a larger protein diameter (~16 nm), β-Gal fills the space between GOx and HRP more completely than NTV (~ 6 nm diameter), resulting in a more enhanced activity for the β-Gal bridge even with a lower co-assembly yield. This result supports the notion that surface-limited diffusion of H_2O_2 between closely-spaced enzymes is responsible for the increase in cascade activity beyond what is possible by three-dimensional Brownian diffusion.

5. Design and construction of responsive DNA nanotweezers with control of inter-component spatial arrangement.

The functions of regulatory enzymes are essential to modulating cellular pathways. We demonstrated a tweezer-like DNA nanodevice to actuate the activity of an enzyme/cofactor pair. A dehydrogenase and NAD^+ cofactor are attached to different arms of the DNA tweezer structure and actuation of enzymatic function is achieved by switching the tweezers between open and closed states. The enzyme/cofactor pair is spatially separated in the open state with inhibited enzyme function, while in the closed state enzyme is activated by the close proximity of two molecules. The conformational state of the DNA tweezers is controlled by the addition of specific oligonucleotides that serve as the thermodynamic driver (fuel) to trigger the change. Using this approach, several cycles of externally controlled enzyme inhibition and activation are successfully demonstrated. This principle of responsive enzyme nanodevices may be used to regulate other types of enzymes and to introduce feedback or

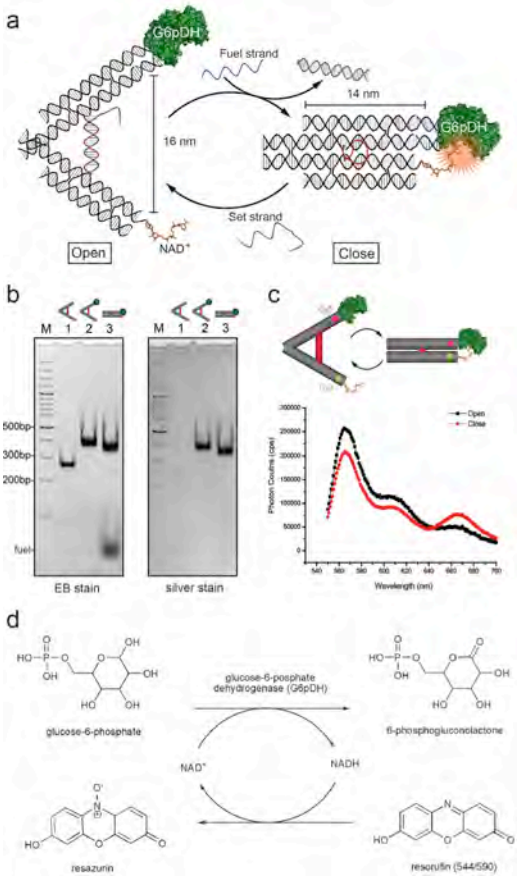

Figure 16. Design and characterization of G6pDH/NAD^+ – assembled DNA tweezers. (a) Schematic illustration of the mechanics of the DNA tweezer-regulated enzyme nanoreactor. (b) Characterization of the fully assembled tweezers structures. (c) Fluorescence energy transfer measurements (FRET) experiment (Cy3/Cy5 dyes) to characterize the open and closed states of the tweezers. (d) Detection of enzymatic activity in the G6pDH/NAD^+-assembled tweezers using a PMS/resazurin coupled assay.

feed-forward control loops.

5.1. The design of DNA tweezers.

The mechanics of the DNA tweezer-regulated enzyme nanoreactor are shown in Figure 16a. A 25 nucleotide (nt) single stranded DNA (ssDNA) oligomer (5'-TTTGCGTAAGACCCACAATCGCTTT-3') connects the ends of the tweezer arms and serves as a structural regulatory element to control the state of the tweezers. In the initial closed state the regulatory oligomer is designed to adopt a 'GCG' stem-loop hairpin structure that holds the two arms of the tweez ers close together. The average distance between the arms in the closed state is ~ 6.9 nm, according to fluorescence energy transfer measurements (FRET). The open s tate is achieved by disrupting the hairpin via hybridization of a complementary set strand to it, thereby generating a rigid ~16 nm long double helical domain between the ends of the tweezer arms. To switch back to the closed state a fuel strand that is fully complementary to the set strand is introduced to the system, releasing the regulatory oligomer to a hairpin by a strand displacement mechanism. The open and closed tweezers were also characterized with AFM.

5.2. DNA-conjugated protein and NAD^+.

Next, G6pDH was conjugated to a ssDNA (5'-TTTTTCCCTCCCTCC-3') using the SPDP crosslinking chemistry. The complementary anchor strand was displayed from one of the tweezer arms to capture the DNA-modified G6pDH via sequence specific hybridization. The other arm of the DNA tweezers was functionalized with an amino-modified NAD^+ molecule.

5.3. Characterization of enzyme-tweezers assembly.

The G6pDH/NAD^+-assembled tweezer complex was characterized by native polyacrylamide electrophoresis (PAGE) as shown in Figure 16b. The protein-bound (~ 100 kD for G6pDH) DNA tweezers exhibited reduced mobility in the PAGE gel due to the relatively higher molecular weight. In addition, the closed state tweezers migrated slightly faster than the open state tweezers due to their more compact conformation. The identity of each band in the gel was verified by ethidium bromide (EB) and silver staining, where EB preferentially bound to the DNA and the metallic silver solution of the protein. The expected band

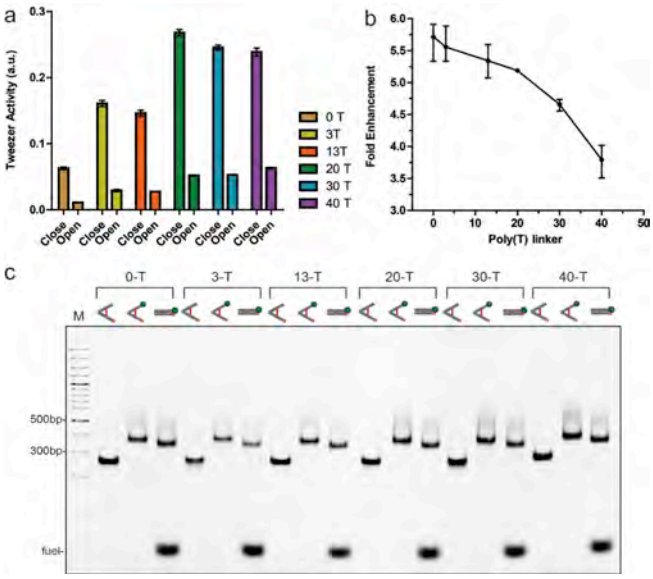

Figure 17. Optimization of the NAD^+ linker length for tweezer activity and actuation. (a) The activities of open and closed tweezers as a function of poly(T) linker length. (b) Enhancement of closed tweezers compared to opened tweezers as a function of poly(T) linker length. (c) Native PAGE characterization of all DNA tweezers with different poly(T) linker length. Slight aggregations of tweezers were observed due to DNA-DNA stacking.

shifts were confirmed by both staining methods. A high yield of enzyme-bound tweezers is visible in the gel images, with evidence of successful switching between open and closed states. As shown in Figure 16c we also characterized the conformational state of the fully assembled tweezers using FRET between Cy3/Cy5 dye pairs. Here, the end of one of the tweezer arms was labeled with Cy3 and the other with Cy5. The closed tweezers exhibited a lower Cy3 signal and a higher Cy5 signal due to relatively efficient energy transfer between the fluorophores. As shown in Figure 16d, a resazurin-coupled assay was used to evaluate the activity of the tweezer bound G6pDH/NAD^+ pair. The assay involves the phenazine methosulfate (PMS) catalyzed reduction of resazurin to resorufin by NADH, as evidenced by the production of a strong fluorescence signal (ex. ~544nm/em. ~590nm). To remove any unassembled enzymes and minimize the background signal all tweezer constructs were purified by biotin-affinity resin treatment.

5.4. Optimization of the activity of enzyme-assembled tweezers.

In an effort to optimize the activity of the G6pDH/NAD^+-assembled tweezers, the NAD^+ cofactor was attached to the tweezers by a single-stranded poly thymidine (T) linker. As shown in Figure 17a and b we investigated the dependence of the length of the poly (T) linker on the activity of the G6pDH/NAD^+-assembled tweezers. Most tweezers were correctly assembled and able to open and close as characterized by native PAGE in Figure 17c. A small amount of aggregation (< 10 %) of the tweezer constructs was observed due to DNA-DNA stacking. The activities of both the open and closed tweezers improved as the length of the linker was increased from 0 to 20 nts (~ 30 nm in linear length), presumably due to the enhanced flexibility of the longer linkers. Further increasing the linker length from 20 nts to 40 nts (~ 60 nm in linear length) did not improve the enzyme activity, but rather resulted in slight decrease. We also evaluated the ability of the tweezers to modulate enzymatic activity by determining the relative level of enhancement of the closed state compared to the open state. As shown in Figure 17b, greater than 5.5-fold activity enhancement was observed for closed tweezers with no linker, or with a short poly $(T)_3$ linker. As the length of the linker increased the enhancement in the activity of the closed tweezers compared to the open tweezers gradually decreased. Tweezers

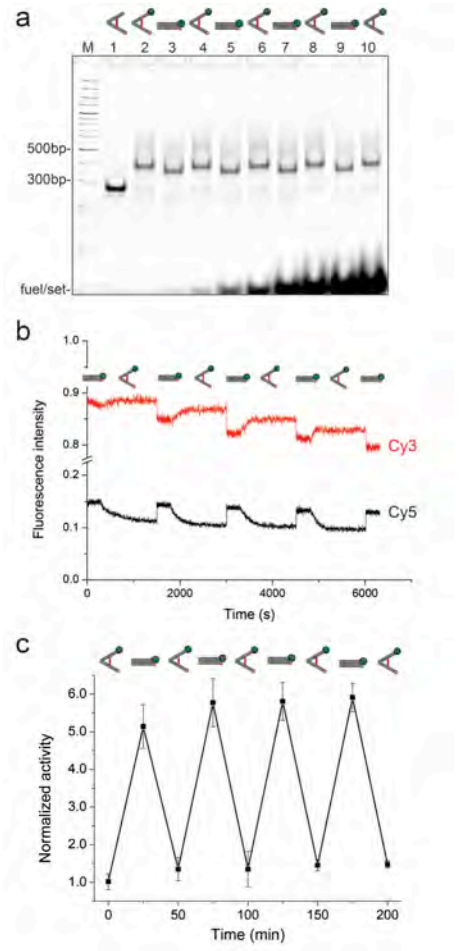

Figure 18. Regulatory cycling of the G6pDH/NAD^+-assembled tweezers. Four cycles of conformational and functional transition were measured and analyzed using (a) native PAGE; (b) real-time FRET and (c) enzymatic assay. Cycles were initiated in the open state, and for each conformational change 50% excess fuel or set strands were added. All the enzyme activities were normalized to the activity of initial open tweezers.

with a relatively long poly $(T)_{40}$ linker exhibited less than 4-fold activity enhancement. This is likely because longer linkers increase the accessibility of NAD^+ to G6pDH even in the open state, thereby reducing the ability of the tweezers structure to modulate enzyme activity. We selected a poly $(T)_{20}$ linker for attachment of the NAD^+ cofactor to the tweezers, which yielded more than 3-fold higher enzymatic activity than tweezers with no linker, and maintained greater than 5-fold activity enhancement of closed tweezers compared to open ones. In this way were able to sustain adequate enzyme activity while also preserving the regulatory capacity of the tweezers.

5.5. Regulatory cycling of the enzyme-assembled tweezers. We further examined the ability of the G6pDH/NAD^+ tweezers to withstand several cycles of on/off enzyme activity. In Figure 18a we present a native PAGE gel that demonstrates the ability of the assembled tweezers to switch between open and closed states 9 times while maintaining their structural integrity. Additional cycles are limited by the accumulation of large amounts of set and fuel strands. We also monitored the real-time opening and closing of the tweezers by labeling the tweezer arms with Cy3 and Cy5 FRET dyes, respectively. As shown in Figure 18b, Cy3 emitted less fluorescence in the closed state due to energy transfer to Cy5, while Cy5 exhibited higher emission under the same conditions. The gradual decrease in the intensity of Cy3 fluorescence over time that was observed can be attributed to photo bleaching. Real time kinetic analysis revealed that the tweezers switch from open to closed states very quickly, with all tweezers transformed within a few seconds (too fast to measure the kinetic constant accurately). However, the kinetics of switching from the closed to open state is much slower, with a first-order kinetic constant of ~ 0.0025 ± 0.0003 s^{-1}. The rate constants corresponding to switching from the closed to open state gradually increased as the cycle number increased: ~ 0.0051 s^{-1} for the second cycle; ~ 0.0054 s^{-1} for the third cycle; and 0.0071 s^{-1} for the fourth cycle. It is likely that the relatively sluggish process of tweezer opening is due to the slow hybridization of the set strand to the self-folded hairpin structure connecting the tweezer arms and the subsequent disruption of the rather stable hairpin structure. The results in Figure 18c demonstrate the ability of the DNA tweezer structure to regulate G6pDH activity by switching between open and closed states. The tweezers were able to actuate the on/off enzyme activity 8 times in 200 minutes, with the closed state producing 5-fold higher enzymatic activity on average than the open state.

In summary, we have designed and constructed a DNA tweezer-like nanostructured enzyme system with the ability to turn on and off the activity of a G6pDH/NAD^+ enzyme/cofactor pair by means of nano-mechanical control. In the open state the tweezer conformation inhibits the activity of the G6pDH/NAD^+ enzyme/cofactor pair by holding the molecules apart, while in the closed state the close proximity of the pair results in greatly enhanced activity. We successfully demonstrated several cycles of enzyme inhibition and activation in response to external stimuli (regulatory DNA strands). With additional developments in DNA-protein/cofactor attachment chemistry it should be possible to regulate other types of enzymes and to introduce feedback or feed-forward control loops. In the future it may be feasible to develop responsive enzyme nanodevices as highly specific chemical amplifiers in diagnostic applications or as biocatalysts in the production of high value chemicals and smart materials.

6. Optimization of the regulatory element of DNA nanotweezers to improve their stability and activity

6. 1. Optimization of DNA nanotweezer design and AFM quantification:

In our design of the above tweezer-like DNA nanodevice to regulate the activity of an enzyme/cofactor pair, the conformational state of the DNA tweezer structure is controlled by the introduction of specific oligonucleotides that serve as the thermodynamic driver (fuel) to trigger the change. To improve the regulation efficiency, we have optimized the original design and we aim to achieve the following two specific goals: (1) quantitatively characterize the conformational changes of DNA tweezers during their operation by AFM measurement, and (2) improve the design of DNA tweezers upon bulk enzymatic measurements to achieve optimal control over the activity of the enzyme/cofactor pair. Firstly, we characterized the original DNA tweezer design containing a hairpin linker with a 3T spacer and 3-bp stem (3T3bp, Figure 19B) as the major regulatory element.

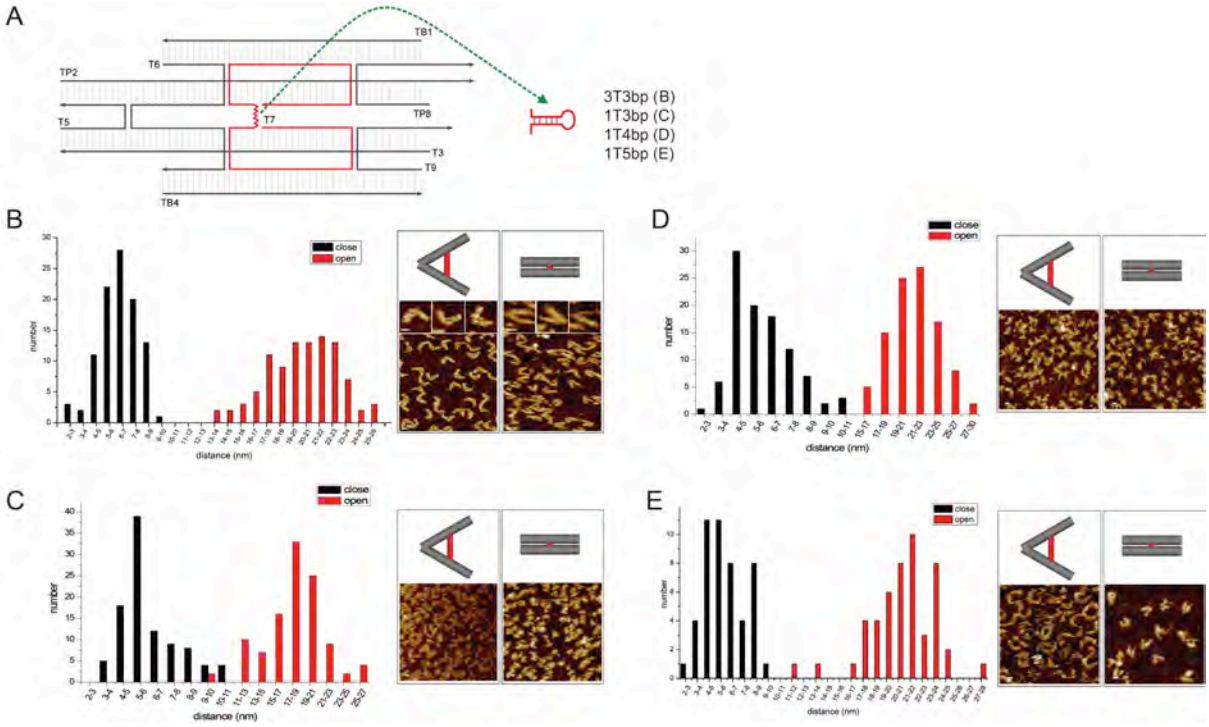

Figure 19. Design of G6pDH/NAD+-assembled DNA tweezers. Schematic illustration of the mechanics of the DNA tweezer-regulated enzyme nanoreactor: a regulatory oligomer (shown in red) is designed to adopt a 'GCG' stem-loop hairpin structure that holds the two arms of the tweezers close together. The addition of a set strand (complementary to the regulatory loop shown in red) to the tweezer structure results in the formation of a DNA double helix between the tweezer arms that separates the G6pDH and NAD+ enzyme/cofactor pair (open state). Displacement of the set strands from the regulatory loop by fuel strands leads to the active state (closed) in which G6pDH and the cofactor NAD+ are in close proximity. AFM scale bar: 10 nm.

The average closed distance between anchoring points of G6pDH and NAD^+ cofactor is 6-7 nm which gave a relatively low FRET efficieny due to the partial closing in the previous report. We hypothesized that replacing this linker sequence by one containing a longer hairpin could increase enzyme activity by bringing the enzyme and cofactor in closer proximity. To this end, we reduced the spacer to a single thymine (1T) and varied

the stem length from 3 to 5bp (1T3bp, 1T4bp and 1T5bp, Figure 19C-D). From the AFM measurements we demonstrated that shortened spacer and increased stem length decreases the distance between two anchoring points to 4-5 nm (Figure 19D and E) and still maintain a good opening distance to 21-23 nm (Figure 19D).

6.2. Functional evaluation of optimized tweezer design:

The G6pDH/NAD^+-assembled tweezer complex was characterized by native polyacrylamide electrophoresis (PAGE) as shown in Figure 20A. The protein-bound (~ 100 kD for G6pDH) DNA tweezers exhibited reduced mobility in the PAGE gel due to the relatively higher molecular weight. In addition, the closed state tweezers migrated

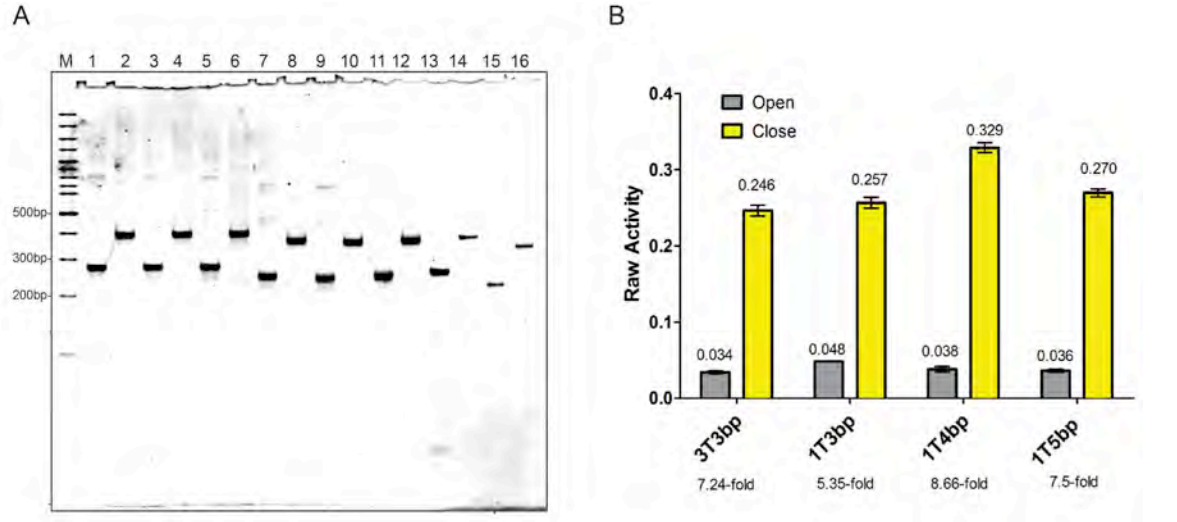

Figure 20. Characterization of G6pDH/NAD^+ – assembled DNA tweezers with different optimized designs. (A) EB stained PAGE gel for assembly of open and closed tweezers. The lower bands are all tweezer controls before assembly with G6pDH. Lanes 1, 3, 5 and 13 represent open tweezers of the original 3T3bp design (1), optimized 1T3bp (3), 1T4bp (5) and 1T5bp (13) respectively; lanes 2, 4, 6 and 14 represents open tweezers assembled with G6pDH; lanes 7, 9, 11 and 15 represent closed tweezers of 3T3bp (7), 1T3bp (9), 1T4bp (11) and 1T5bp (15) repectively; lanes 8, 10, 12 and 16 represent closed tweezers assembled with G6pDH. (B) Enzyme activities of the original 3T3bp design and optimized 1T3bp, 1T4bp, 1T5bp designs. Yellow bar shows the activity at closed state and grey bar represents the activity at open state.

slightly faster than the open state tweezers due to their more compact conformation. The identity of each band in the gel was verified by ethidium bromide (EB). The enzyme activity of assembled G6pDH/NAD^+ structures was evaluated using previously a reported PMS/resazurin coupled assay: NAD^+ is first reduced to NADH by G6pDH. Next, PMS catalyzes electron transfer from NADH to resazurin, producing the strongly fluorescent compound resorufin, which has an emission maximum ~ 590 nm when excited at 540 nm. Raw activity and fold enhancement is shown in Figure 20B. 1T4bp design shows enhanced activity at closed state while still maintaining a relatively low activity at open state. Shortening the spacer to 1T and enlogating the stem to 4bp provides optimal closing distance as well as increased fold enhancement compared to the original 3T3bp tweezer.

7. Demonstrating the ability of DNA nanocages to encapsulate multi-enzyme cascades.

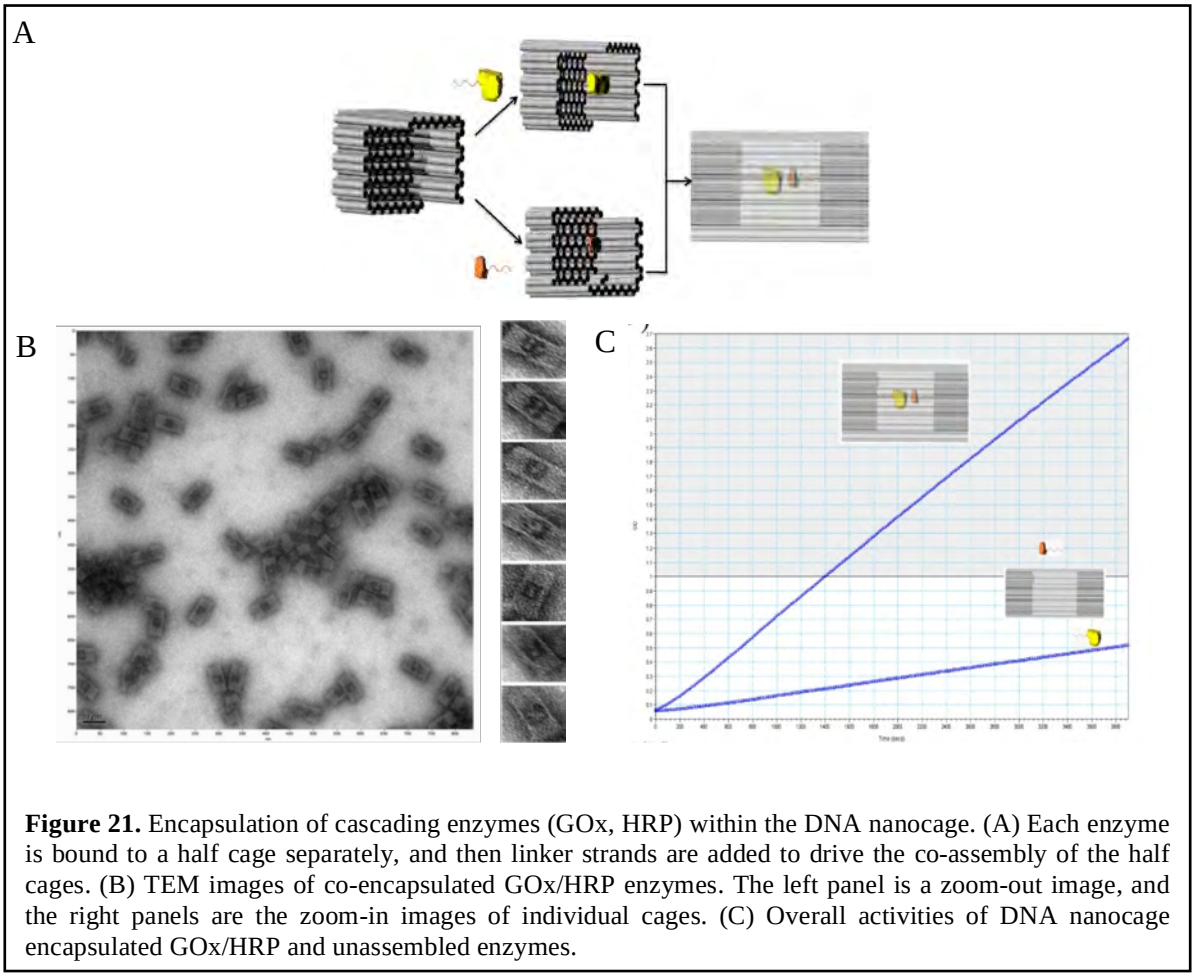

Figure 21. Encapsulation of cascading enzymes (GOx, HRP) within the DNA nanocage. (A) Each enzyme is bound to a half cage separately, and then linker strands are added to drive the co-assembly of the half cages. (B) TEM images of co-encapsulated GOx/HRP enzymes. The left panel is a zoom-out image, and the right panels are the zoom-in images of individual cages. (C) Overall activities of DNA nanocage encapsulated GOx/HRP and unassembled enzymes.

We designed and constructed a DNA nanocage system where two half-cages are co-assembled to form the complete cage depicted in Figure 21. We utilized this cage to encapsulate a GOx/HRP enzyme cascade. In Figure 21, GOx and HRP were attached to complementary half-cages and the subsequent interaction between the two half-cages directed the co-encapsulation of GOx/HRP within the closed cage. In Figure 21 C, the encapsulated enzymes showed ~ 5-fold enhancement in activities as compared to free enzymes.

8. Demonstration of the open and close of DNA nanocages.

To build DNA nanocage encapsulated enzyme nanoreactors that can respond to external cues. We successfully constructed a DNA nanocage

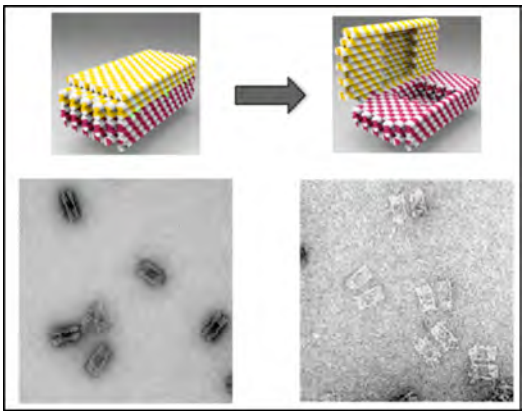

Figure 22. Schematic illustrating a DNA nanocage with a locking mechanism that is opened by external DNA signals, with TEM images of the closed and open boxes shown below.

with a molecular lock mechanism that is unlocked by an external DNA key. The DNA nanocage containing the lock strands are formed using the DNA origami technique where protruding unhybridized DNA oligos serves as a key and a strand displacement technique is used to dehybridize and unlock the cage through specific DNA oligos serving as the key. The nanocage opening is highly efficient and we are in the process of using this to regulate the encapsulated enzymes and control their activities.

V. Publications & Patents

1. A. Pinheiro, D. Han, W. M. Shih, and H. Yan, Challenges and Opportunities for Structural DNA Nanotechnology. ***Nature Nanotechnology***. 6, 763-772, 2011.
2. J. Fu, M. Liu, Y. Liu, and H. Yan, Spatially-Interactive Biomolecular Networks Organized by Nucleic Acid Nanostructures, Acc. Chem. Res. 45, 1215-1226 (2012).Jinglin Fu & Hao Yan "Controlled drug release by a nanorobot", ***Nature Biotechnology*** 2012, *30*, 407–408.
3. J. Fu, M. Liu, Y. Liu, N. W. Woodbury, and H. Yan, Interenzyme Substrate Diffusion for an Enzyme Cascade Organized on Spatially Addressable DNA Nanostructures, ***J. Am. Chem. Soc***. 134, 5516–5519 (2012).
4. D. Han, S. Pal, Y. Yang, S. Jiang, J. Nangreave, Y. Liu, and H. Yan. DNA Gridiron Nanostructures Based on Four-Arm Junctions, ***Science,*** 339, 1412-1415 (2013).
5. M. Liu, J. Fu, C. Hejesen, Y. Yang, N. W. Woodbury, K. Gothelf, Y. Liu, and H. Yan, A DNA Tweezer-Actuated Enzyme Nanoreactor, ***Nature Comm.***, 4:2127 (2013).
6. F. Zhang, J. Nangreave, Y. Liu, H. Yan, Structural DNA Nanotechnology: State of the Art and Future Perspective, ***J. Am. Chem. Soc.***, 136, 11198–11211 (2014).
7. J. Fu, Y. R. Yang, A. Johnson-Buck, Y. Liu, N. G. Walter, N. W. Woodbury, and H. Yan, Multi-enzyme Complexes on DNA Scaffolds Capable of Substrate Channeling with an Artificial Swinging Arm, ***Nature Nanotechnology***, 9, 531-536 (2014).
8. DNA Gridiron, Inventors: Dongran Han & Hao Yan, Provisional patent filed, 2014.

VI. Invited talks and conference presentations

From Hao Yan:

1. "Designer DNA Nanoarchitectures for Programmable Self-assembly", 40th Annual Naff Symposium on Chemistry and Molecular Biology, April 25, 2014. (Keynote speaker).
2. "Designer DNA Nanoarchitectures for Programmable Self-assembly", Department

of Chemistry, U. of Michigan, April 1, 2014.

3. "Designer DNA Nanoarchitectures for Programmable Self-assembly", Department of Chemistry, U. of Chicago, March 31, 2014.
4. "New Innovations in Biotechnology: Molecular Design and Biomimicry", Presidential Engagement Program, Building Solutions to Grand Challenges: Creating Societal Impact Through Use-Inspired Research, Arizona State University, March 13, 2014.
5. "Designer DNA Architectures for Programmable Self-assembly", Bio-Inspired Computing: Theories and Applications 2013 (BIC-TA 2013), Huangshan, China, July 12-14, 2013. (Keynote speaker).
6. "Designer DNA Architectures for Programmable Self-assembly", 10th Annual Conference, Foundation of Nanoscience, Self-assembled Achitectures and Devices, Snowbird, Utah, April 15-18, 2013. (Keynote speaker)
7. "Designer DNA Architectures for Programmable Self-assembly", Wyss Institute of Bioinspired Engineering, Harvard University, May 13, 2013.
8. "Designer DNA Architectures for Programmable Self-assembly", Department of Bioengineering, MIT, May 9, 2013.
9. "Designer DNA Architectures for Programmable Self-assembly", Department of Chemistry, Penn State Univ, April 3, 2013.
10. "Designer DNA Architectures", DNATEC workshop, Arhus, Denmark, August 13, 2012.
11. "Designer DNA Nanostructures for Nanobiotechnology", Biochemistry and Molecular Pharmacology, University of Massachusetts Medical School, Worcester, MA, May 9, 2012.
12. "Designer DNA Nanostructures", Department of Chemistry, University of Nebraska - Lincoln, NE, April 6, 2012.
13. "Designer DNA Nanostructures", Seminar Series in Chemical Biology, Yale University – New Heaven CT, April 4, 2012.
14. "Designer DNA Architectures for Nanotechnology", the 243rd ACS National Meeting, San Diego, CA, March 25, 2012.
15. "Designer DNA Architectures", DNA Nanotechnology Conference: From Structure to Function, Shanghai, China, March 16-19, 2012.
16. "Designer DNA Nanostructures", the 14th IUPAC conference on Polymers and Organic Chemistry, Doha, Qatar, Jan. 6-9, 2012.
17. "Designer DNA Nanostructures", the 17th International Conference on DNA Computing and Molecular Programming, Pasadena, CA, Sept. 19-23, 2011. (Plenary Talk).

From Yan Liu:

18. “Hybridization Kinetics of Higher-Order DNA Assemblies”, A. V. Pinheiro, J. Nangreave, H. Yan, Y. Liu. DNA 17, Pasadena, CA, July, **2011.**

19. “DNA Gridiron”, D. Han, Y. Liu, H. Yan. FNANO12, Snowbird, Utah, April, **2012.**

20. “Nucleic Acid Driven Polypeptide Assembly” J. Flory, S. Shinde, Y. Liu, H. Yan, G. Ghirlanda, P. Fromme, FNANO13, Snowbird, Utah, April, 2013.

21. “Self-assembly of Archimedean DNA Structures” F. Zhang, H. Yan, Y. Liu, FNANO13, Snowbird, Utah, April, 2013.

22. “Hybridization Kinetics of Multivalent DNA Tiles” Shuoxing Jiang, Dongran Han, Hao Yan and Yan Liu, DNA 19, Tempe, AZ, 2013.

23. “DNA Nanoarchitectures”. Yan Liu. Albany 2013: Conversation 18, June 2013.

24. “DNA Directed Light Harvesting Antenna System to Enhance and Control the Absorption Cross-section of Photosynthetic Reaction Center”. Palash K. Dutta, Su Lin, Andrey Loskutov, Symon Levenberg, Daniel Jun, Rafael Saer, J. Thomas Beatty, Yan Liu, Hao Yan, Neal Woodbury. FNANO14, Snowbird, Utah, April, 2014.